EXPERIMENTAL INVESTIGATION OF FORCED-CONVECTION HEAT TRANSFER IN WAVY CHANNELS

Luigi Colombo, Adriano Muzzio, Alfonso Niro

Dipartimento di Energetica, Politecnico di Milano, I-20133 Milano, Italy

ABSTRACT

This paper presents experimental data on heat transfer coefficients and pressure drops of air-flows through two different wavy channels at Reynolds numbers ranging between 500 and 7000; data for a plain channel are also reported for comparison. All the channels have a rectangular cross-section, 10 or 15 mm high and 200-mm wide; the wavy channels exhibit the lower and upper walls corrugated by triangular cross-section relieves arranged perpendicularly to the flow direction and staggered on the two walls. Local fluid dynamics and heat transfer characteristics are investigated by means of not-intrusive, optical techniques for Reynolds number up to 1800, whereas data on average heat transfer coefficient and pressure drop over the whole channel are obtained by conventional, intrusive measurements. In laminar flow the heat transfer enhancement with respect to the plain channel is poor as it ranges from 10% to 30%, while it becomes a quickly increasing function of the Reynolds number when flow regime starts to be transitional (Re≈1300), and it comes up to near 4 at Re=7000; pressure drops, however, exceed by 2-3 times the plain channel values in laminar flow and even by 10 times in turbulent flow.

INTRODUCTION

Air-flows inside narrow rectangular channels are frequently encountered in compact heat exchangers with extended surfaces and in microelectronic packages. Due to the small passages and the relatively low air velocity, flow is laminar or weakly turbulent and, therefore, convective coefficient is low. When enhanced heat transfer is desired, specially configured extended surfaces, such as offset strip, louvered, perforated, and wavy ribs, are largely employed because they increase convective coefficient from 50 to 150% while keeping cost-effectiveness and reliability. The heat transfer augmentation is obtained mainly by altering the duct fluid-dynamic rather than by increasing the surface. Many enhancement mechanisms have been explored; however, the most frequently used are periodic deflection of streamlines, periodic interruptions of the boundary layer growth and flow destabilization. Furthermore, corrugations also promote turbulence development, since their size is close to that of the structures to be excited (the lower the Reynolds number, the larger these structures). As the shape of these specially configured fins depends on the enhancement mechanisms employed, there is a large variety of geometries and, consequently, a large number of studies in the open literature. For instance, Webb (1994) reports more than 35 papers and almost as many are cited by Fiebig (1996). For offset strip fin geometry, correlations for predicting the Colburn and friction factors were proposed by Kays (1972), Joshi and Webb (1987), and Wieting (1975); similar correlations were developed by Davenport (1984) for louvered fin geometry. Finally, wavy fin geometry is also the subject of some interesting studies, such as those by Goldstein and Sparrow (1977) and Ali and Ramadhyani (1992), but there are not quite general correlations for this geometry because of a rather lacking data base. For these motivations, we are currently performing an experimental and numerical investigation on flows through channels with wavy walls.

This paper reports on heat transfer characteristics of air-flows inside two channels with the upper and lower walls wavy configured, at Reynolds numbers encompassing laminar-, transitional- and weakly turbulent-flow regime. Waviness have a triangular cross-section of 20-mm width and of 2.68-mm height; in a channel, which we refer to as the type A channel, relieves alternate with 10-mm long, flat strips so the relief apex on a wall coincides with the strip middle point on the other one, whereas in the other channel (type B) they follow one another staggered on the lower and upper walls. Both types of waviness induce a periodic deflection of the streamlines resulting in a heat transfer enhancement and, ineluctably, in higher pressure drops. Local fluid dynamics and heat transfer coefficients are experimentally investigated for Reynolds numbers up to 1800 by not-intrusive measurements of velocity fields and of temperature, or temperature-gradient, fields by means of laser Doppler velocimetry, real-time holographic-interferometry and digital speckle-photography, respectively. Finally, data on average heat transfer coefficient and pressure drop are obtained all over the investigated range of Reynolds number by conventional measurements.

EXPERIMENTAL SETUP AND MEASUREMENT TECHNIQUES

The experimental setup consists of two independent circuits, namely, the air circuit containing the test section, and the heating-water circuit. Through an opening with rounded surfaces, room air flows into an entry-section, that is a rectangular duct, with the same transverse dimensions as the test section, of 1-m length, i.e., 30 times the hydraulic diameter;

the entry-section walls are not heated. At the end of this duct, fully developed flow condition is reached and air enters the test-section. This is a 200-mm wide, 800-mm long channel of 10- or 15-mm height. The test-section side-walls are glass windows to allow optical access to its inside; the lower and upper walls are manufactured with aluminum blocks, mounted side by side and strongly tightened to the heating channel, where water flows in opposite direction of the air. To check if temperature is uniform over the heated walls, six thermocouples are embedded in the lower wall and two in the upper one; each thermocouple is cemented in a blind hole with the tip placed 0.5 mm from the wall surface. Downstream the test-section, there are a 0.5-m long exit-section, a filter, three float-type flow-meters, a metering valve and a blower operating in suction mode; the exhausted air is discharged outside the laboratory. The heating circuit is mainly composed by a heat bath, with a high precision controller, which provides a high mass flow-rate of water at constant temperature. Air temperature is measured at the test-section inlet, downstream the filter, and upstream and downstream the flow-meters.

Local fluid dynamics and heat transfer characteristics are not-intrusively investigated. Air velocity is measured by laser Doppler velocimetry by means of a TSI system including a fiber-optic probe and the IFA750 signal processor. Velocity is measured along vertical traverses, 2 or 5 mm apart each other; for every traverse, measurements are taken in 15-20 points; finally, each measurement is the average of five readings based on a 1024 data sample.

Temperature fields are measured by real-time holographic-interferometry. A two-beam interferometer is used with a He-Ne laser of 35-mW power as light source. The reference state of the air flow, corresponding to the experimental setup at the room temperature, is first recorded on a photographic plate; the plate is then processed and accurately repositioned into its original location by means of electrostrictive micro-positioners. Finally, the reference state is reconstructed by illuminating the plate, while the convective heat transfer phenomena to be investigated occur, and this results in a real-time interference. Principles and methods of the holographic interferometry are reported in Vest (1979). Interferograms are electronically recorded by a monochrome, progressive-scan, ½"-CCD camera with 760×530 pixel resolution, 10-bit dynamic range, at 25 not-interlaced fps rate. The evaluation of interferometric images consists in reconstructing the phase-difference distribution from the light-intensity distribution; this has been performed by using either the classic method based on maximum/minimum fringe location (Hauf and Grigull, 1970) or a phase-shifting method (Carré). Once the phase-difference distribution has been determined, the temperature field is evaluated by the ideal-interferometry equation. Temperature profiles are obtained over 20-30 vertical traverses equally spaced along a corrugation pitch, included ones where velocity profiles have been taken (thus the bulk temperature can also be calculated).

Temperature-gradient fields are measured by means of another optical technique, i.e., the double-exposure digital speckle-photography, based on evaluating speckle displacement between the object and reference exposures, as described by Fomin (1998). In this study, we adopt an experimental set-up where speckle patterns are generated by an optical system, i.e., a "subjective speckles" arrangement, because it should provide a higher spatial resolution and a wider measurement range, as discussed by Jones and Wykes (1983); speckle patterns are digitally recorded by means of the CCD camera previously described. As the channel-flow field shot is only of 640 μm × 446 μm, a scanning along the vertical traverses camera is required; to do this, optics are assembled in a rigid probe and mounted on a two-axis, 5-μm accuracy shifting-system. Speckle displacement is determined by searching the position where the cross-correlation function between the object and reference exposures has the maximum. Finally, the cross-correlation function is calculated on five consecutive sub-domains of 106×106 pixels, centered on the mean line; this dimension is about ten times greater than the maximum speckle-displacement and therefore is large enough to disregard speckle-pattern decorrelation due to speckles displacing out of the calculation domain.

Average heat transfer coefficient and pressure drop over the full test-section are also investigated but not simultaneously with local characteristics because their measurement is intrusive. The average Nusselt number over the test-section is calculated as

$$Nu_m = \frac{\rho \Gamma_v c_p D_h}{k A_s} \ln \frac{\theta_i}{\theta_o} \qquad (1)$$

where Γ_v is the air volume flow rate, ρ the density calculated at temperature and pressure where Γ_v is measured, c_p specific heat at constant pressure, k thermal conductivity, A_s heated-surface total area , θ_i and θ_o the wall to air-bulk-temperature difference at the inlet and outlet of the test-section, respectively. To measure the air outlet-bulk-temperature, the exit-section is equipped with two rows of turbolizers and a convergent section that conveys air flow through a narrow duct of 1-cm width; this duct is filled with a tangle of metallic fine wires and two thermocouples are embedded inside. The uncertainty on Nu_{av} measurement, based on a propagation error analysis, is 6% on the average but it becomes larger than 15% when θ_o lowers under 2 °C, namely, at the highest values of Nu_{av}.

Pressure drop is measured by means of two probes plugged into the channel through the air entrance, and connected to a differential micromanometer of 0.125-Pa sensitivity; each probe consists of a 6-mm o.d., 1500-mm long tube with a closed, rounded tip, and with two pairs of 0.1-mm-diameter, pressure taps drilled on the tube side at 2-cm from the tip. The apparent Darcy friction factor is calculated as

$$f = \frac{2 D_h A^2}{\rho \Gamma_v^2} \frac{\Delta p}{L_c} \qquad (2)$$

where Δp is the pressure drop over the whole wavy channel, A and L_c are the cross section area and the length of the channel, respectively. The measurement of this factor is affected by an uncertainty of 5.2% on the average but it comes up to 10% at the lowest values of Δp.

RESULTS AND DISCUSSION

The geometry of the channels investigated in this paper is schematically showed in Fig. 1 whereas Tab. I lists their main characteristic parameters.

The Fig. 2 shows the streamwise distribution of the local Nusselt number along both the lower and upper walls of the channel A, for Reynolds numbers of 500 and 1250. Data are taken in the region around the seventh corrugation of the lower wall where velocity measurements have assessed that flow is periodically fully developed.

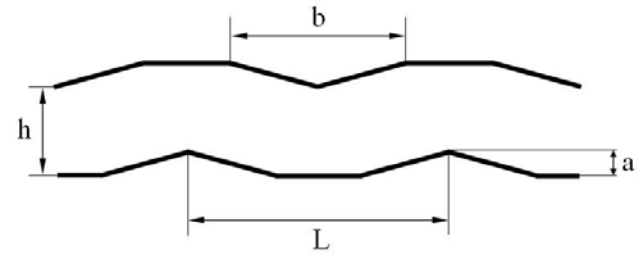

Channel A

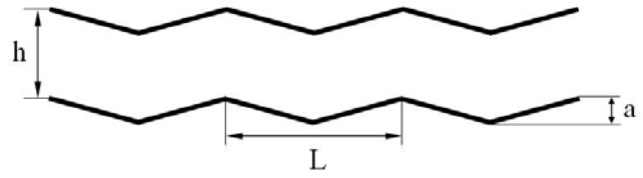

Channel B

Figure 1. Geometry of the channels.

Parameter / Channel		A	B
h	[mm]	15	10
a	[mm]	3	3
b	[mm]	20	-
L	[mm]	30	20
Width	[mm]	200	200
Hydraulic diameter	[mm]	27.9	19.0
Ribs number		25	30

Table 1. Main geometrical parameters.

Data for the upper wall are plotted downstream translated of half a pitch for a better comparison; this transposition is allowed if flow is also thermally fully-developed and, as will be shown later on, this condition is actually satisfied. The figure also reports the limiting value of the Nusselt number for fully-developed laminar flow in a rectangular duct with two isothermal and two adiabatic walls; this value is 6.68 and is obtained by interpolating data reported by Shah and London (1978). Inspection of the figure shows that the local Nusselt number increases along the windward side, it reaches a maximum on the corrugation edge with a value up to four times higher than the plain channel, and then it starts to steeply decrease. In the valley, due to the presence of a large separation bubble, the Nusselt number results well below the per-module-average value, and it is even lower than the plain-channel value. The difference between the Nusselt numbers on the corrugation peak and in the valley increases with the Reynolds number, but the per-module-average value only slightly exceeds the plain-channel value in this range of Reynolds numbers. Finally, the good matching of experimental data at the ends of the corrugation pitch confirms the assumption that flow is thermally, periodically fully-developed.

Streamwise distributions of local Nusselt number inside the channel B for Reynolds number ranging from about 500 and 1750 are shown in Fig. 3. The measurement region lies on the thirteenth corrugation of the lower wall, 250-mm downstream of the test-section inlet, where periodically fully-developed flow conditions are attained as well as in the previous case.

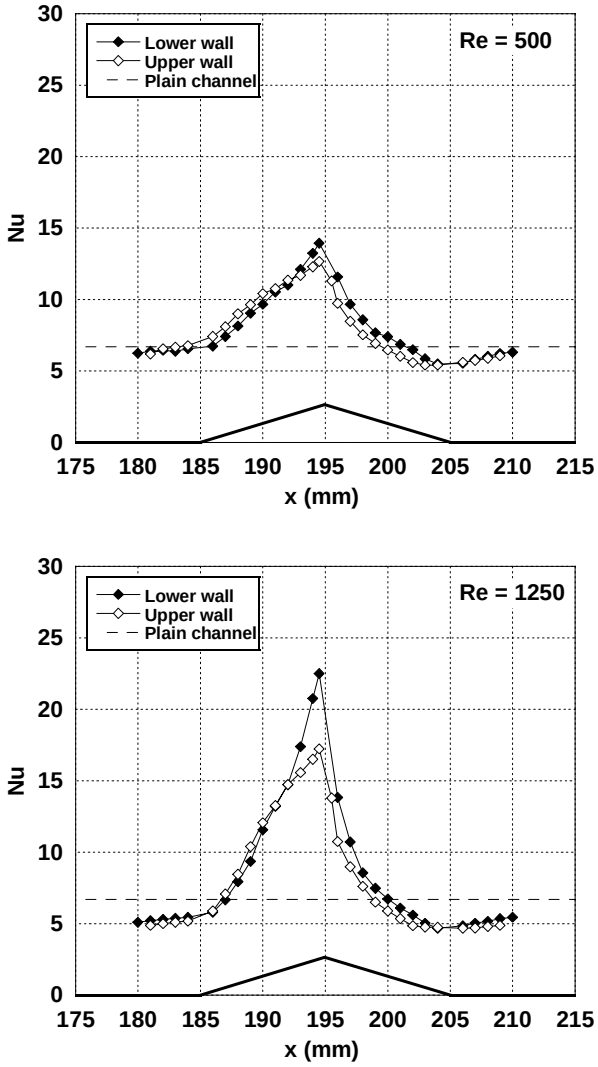

Figure 2. Local Nusselt number distribution for channel A.

Temperature-gradient measurements are taken along six vertical lines, at 12 locations equally spaced of 0.9 mm; if needed, spacing is halved close to the boundaries. The experimental points taken on the upper side are plotted translated of half a pitch, i.e., ahead of the data for the lower side as if they had been obtained along the windward facet of the thirteenth lower corrugation. The distributions are relative to three different Reynolds numbers, i.e., 480, 1370 and 1750. As it can be seen, the trends are quite similar between them; the local Nusselt number increases along the windward facet, it reaches a maximum on the corrugation edge exhibiting values 2.4, 4.5 and 5.3 times higher than the plain channel, and eventually it starts to decrease at first very quickly and then more slowly while approaching the corrugation trough.

Consideration will now be given on the average heat transfer coefficients and on the pressure drop over the whole test-section. Fig. 4 shows the data of the average Nusselt number plotted versus the Reynolds number; for comparison, the figure also reports as solid lines the values calculated for a plain-channel by the correlations of Shah and London for Re≤2300, and of Gnielinsky for higher values (Kakaç, 1987); all predictions take into account thermal effects of the entry-region. As seen, for Reynolds numbers up to about 1250, both the wavy channels exhibit a Nusselt number essentially constant as the plain channel, but the values are slightly higher, namely, 8.11 for the Channel A and 11.16 for the Channel B, that imply an augmentation of 10% and 25%, respectively. Obviously, these

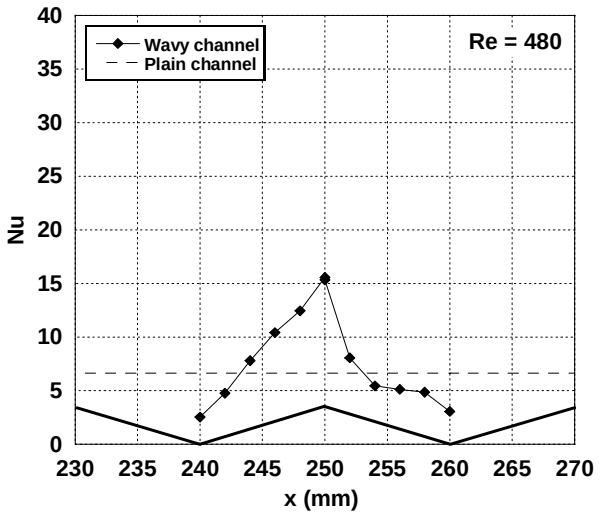

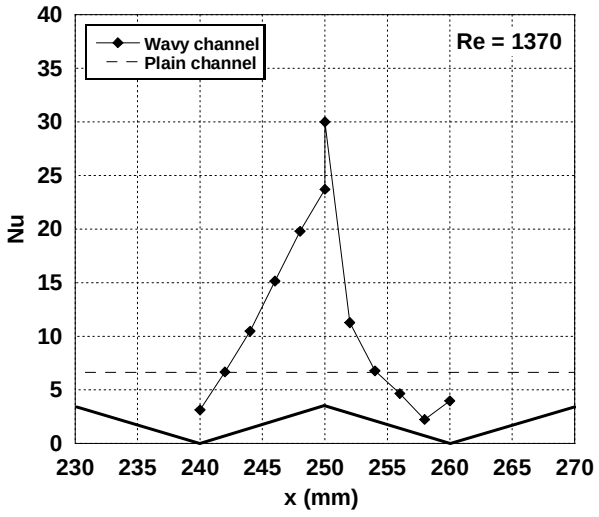

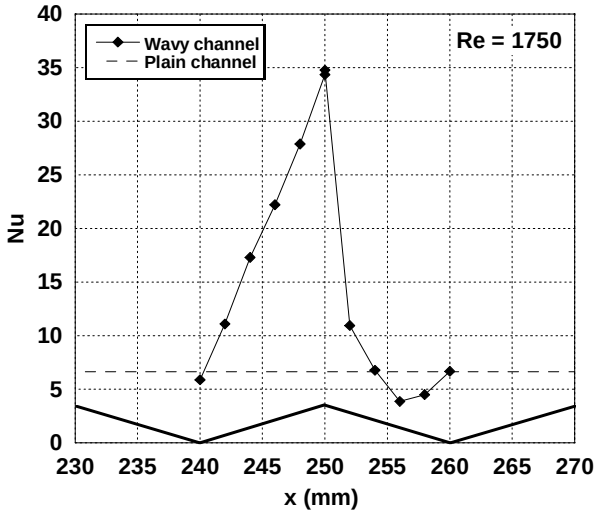

Figure 3. Local Nusselt number distribution for channel B.

values of Nusselt number are also larger than the per-module-average values in the thermally fully developed region, because they benefit of the entry region. Therefore, we can infer that for Re≤1250 flow is laminar, and wall waviness signifycantly alter the distribution of the local Nusselt number but

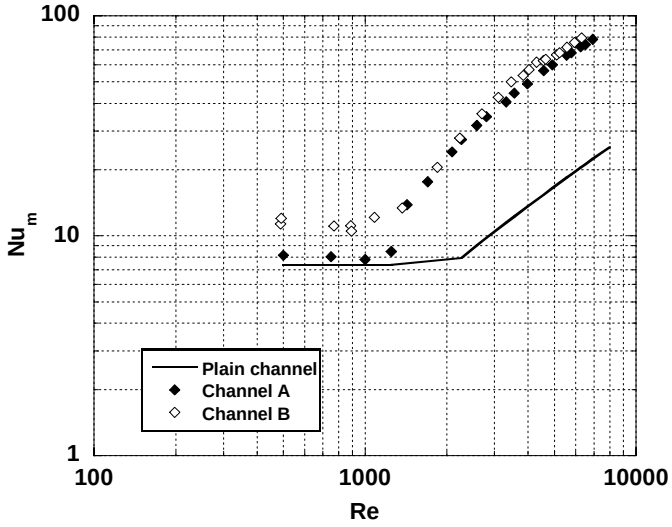

Figure 4. Average Nusselt number versus Reynolds number.

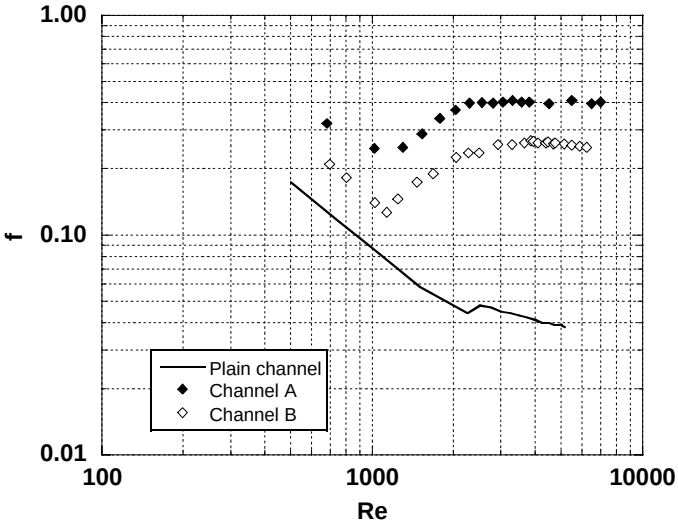

Figure 5. Average friction factor versus Reynolds number.

affect to a much less extent the overall heat transfer characteristics. Similar findings have been reported by Goldstein and Sparrow (1977) and by Ali and Ramadhyani (1992) in their studies on corrugated wall channels.

For Re>1250 data for both channels begin to steeply rise with the Reynolds number, and shortly they fairly overlap. Data exhibit a power-law dependence on the Reynolds number; up to Re=3100, the exponent is 1.43 and after it lowers to 0.8. From this trend we argue that flow is transitional for Reynolds numbers between 1250 and 3100, and after it becomes fully turbulent. At Re=7000, corresponding to the upper limit of the investigated range, the average Nusselt number is 78 with a 400% increase with respect to the plain channel.

Finally, Figure 5 reports the experimental values of the apparent Darcy friction factor plotted versus the Reynolds number for the present channel and, for comparison, for a plain channel with the same width but of 15-mm height. In laminar flow, the friction factor displays for both wavy channels a trend quite similar to the plain channel but with larger values, i.e., 270% for the Channel A and 150% for the Channel B. When the flow becomes transitional, the trend reverses and the

friction factor starts to noticeably increase; as the Reynolds number is further increased, the growth lowers and eventually, when flow is fully turbulent, the friction factor seems to attain an asymptotic value in the channel A, and to reverse again its trend in the channel B. At Re=6300, the values are much higher than the plain channel, i.e., 0.4 and 0.25 for the Channels A and B, respectively. However, as already noticed by other authors as Molki and Yuen (1986), the latter observation should be interpreted with great caution, because of the difference in the hydraulic diameter D_h. In fact, the measured pressure drops per unit length at the same Reynolds number are higher for the channel B than for the channel A which conversely exhibits the highest friction factor; from the definition of the friction factor given in Eq. 2, we may conclude that the larger values for the channel A are indicative of the increased value of D_h rather than of higher pressure drops.

CONCLUSIONS

The paper reports experimental data on local and overall heat transfer coefficients, and on pressure drops as well, inside two wavy channels at Reynolds numbers ranging from 500 to 7000. The overall heat transfer measurements show that flow is laminar up to Re=1250; within this regime, the average Nusselt number is independent on Reynolds number, as for the plain-channel case, but its value is only 10% or 25% higher for the channels A and B, respectively; on the contrary, the local Nusselt number exhibits very far larger variations with respect to the plain channel. In spite to these very poorly enhanced average heat transfer characteristics, however, the Darcy apparent friction factor worsens of 270% and 150% for the Channel A and B, respectively. For Re>1250, flow becomes transitional and, therefore, in advance with respect to the plain channel. This event is well pointed out by a slope change in the average Nusselt number trend which, from a constant, becomes a power-law increasing function of the Reynolds number with an exponent of 1.43. The transitional flow regime is characterized by a strong increase of the heat transfer coefficient, and of the apparent friction factor with respect to the plain-channel. Finally, for Re≥3100 flow becomes fully turbulent, the growth of the average Nusselt number with Re weakens and the exponent lowers to 0.8, i.e., the characteristic value for plain channel. Consequently, both the investigated wavy channels are equally very effective in enhancing heat transfer in turbulent flow irrespectively of geometry; indeed the enhancement factor comes up to 4. However, the heat transfer augmentation is largely penalized by the accompanying increase of the apparent friction factor that for the channel A comes up to 10 times higher than the plain-channel.

AKNOWLEDGMENTS

This work is supported by MURST (the Italian Ministry for the University and for the Scientific and Technical Research) via 2002 PRIN grants.

REFERENCES

1. Ali, M.M., Ramadhyani, S., Experiments on convective heat transfer in corrugated channels, Experimental Heat Transfer, Vol. 5, pp. 175-193, 1992.
2. Davenport, C.J., Correlations for heat transfer and flow friction characteristics of louvered fin, Heat transfer-Seattle 1983, AIChE Symp. Ser., No. 225, Vol. 79, pp. 19-27, 1984.
3. Fiebig, M., Vortices: tools to influence heat transfer. Recent developments, Proc. 2nd European Thermal Sciences and 14th UIT National Heat Transfer Conference, vol. 1 pp. 41-56, Rome, June 1996.
4. Fomin N.A., Speckle photography for fluid mechanics measurements, Berlin, Springer, 1998.
5. Goldstein, L.J., Sparrow, E.M., Heat/mass transfer characteristics for flow in a corrugated wall channel, J. Heat Transfer, Vol. 99, pp. 187-195, 1977.
6. Hauf, W., Grigull, U., Optical methods in heat transfer, in Advances in Heat Transfer, Vol. 6, p. 133, Academic Press, 1970.
7. Joshi, H.M., Webb, R.L., Prediction of heat transfer and friction in the offset strip fin array, Int. Journal of Heat and Mass Transfer, Vol. 30, No. 1, pp. 69-84, 1987.
8. Jones R., Wykes C., Holographic and Speckle Interferometry, Cambridge University Press, 1983.
9. Kays, W.M., Compact Heat Exchangers, AGARD Lecture Ser. No. 57 on Heat Exchangers, ed. Ginoux, AGARD-LS-57-72, Jan. 1972.
10. Molki M., Yuen C.M., Effect of interwall spacing on heat transfer and pressure drop in a corrugated–wall duct, Int. J. Heat Mass Transfer, Vol. 29, No. 7, pp. 987-997, 1986.
11. Kakaç S., Shah R. K., Win A., Handbook of Single-Phase Convective Heat Transfer, John Wiley & Sons, New York, 1987.
12. Vest, C.M., Holographic interferometry, John Wiley & Sons, 1979.
13. Webb, R.L., Principles of Enhanced Heat Transfer, John Wiley & Sons, cap. 9, pp. 228-284, 1994.
14. Wieting, A.R., Empirical correlations for heat transfer and flow friction characteristics of rectangular offset fin heat exchangers, J. Heat Transfer, Vol. 97, pp. 488-490, 1975.